Results in Engineering 23 (2024) 102415

Contents lists available at ScienceDirect

Results in Engineering

journal homepage: www.sciencedirect.com/journal/results-in-engineering

Research paper

A cutting-edge broadband Camembert-inspired dielectric resonator antenna

Kaoutar Allabouche [a,b,c,*], Fabien Ferrero [a], Hugo Bernadac [a], Jean-Marc Ribero [a], Leonardo Lizzi [a], Najiba El Amrani El Idrissi [c], Mohammed Jorio [b], Guillaume De Calan [d], Julien Sourice [d]

[a] Université Côte d'Azur, CNRS LEAT, Sophia Antipolis, 06410, France
[b] Université Sidi Mohamed Ben Abdellah, SIGER-FST Fès, Fès, 30000, Morocco
[c] Université Sidi Mohamed Ben Abdellah, LSSC-FST Fès, Fès, 30000, Morocco
[d] Nanoe Corporation, 6 Rue des Frênes, Ballainvilliers, 91160, France

ARTICLE INFO

Keywords:
Cylincrical dielectric resonator antennas (CDRA)
High permittivity ceramics
Propagation
HFSS
UMTS (universal mobile telecommunications system)
DECT (digital enhanced cordless telecommunications)
Bandwidth enhancement
Additive technologies

ABSTRACT

This article introduces an innovative approach to significantly broaden the bandwidth of Cylindrical Dielectric Resonators. A four-element Camembert-Shaped Cylindrical Dielectric Resonator Antenna (CDRA) is presented, using an air gap separating the resonators to enhance the antenna bandwidth. The radiators, i.e., the DRA blocks, are made of high relative-permittivity ceramic material (ε_r = 25 & 30) and are excited by microstrip-line feed. The proposed methodology involves the strategic design of these resonators, incorporating dielectric materials to finely optimize the frequency response. Experimental validation demonstrates a remarkable improvement in bandwidth when compared to conventional methodologies. This novel technique holds immense promise for applications requiring wideband antennas. The demonstrated effectiveness of this approach not only addresses contemporary challenges but also opens up new avenues in antenna design, catering to the escalating demands of modern communication systems. In addition to the compact dimensions of the elementary radiating element, the separation distance between them, set at $\lambda/4$, enhances the array antenna overall size, and its gain is nearly 10 dBi. The proposed antenna covers cellular network applications such as UMTS mobile phone band around 2.1 GHz, as well as wireless DECT phone bands around 1.9 GHz, facilitating data transmission over short distances and beyond, with an impedance bandwidth of 20%.

1. Introduction

New developments in wireless communications aim to provide global mobility and a variety of services such as phone calls [1][2], internet access and fast data transmission. As cellular communications undergo rapid expansion, antennas for wireless communication need to be compact, wideband, and maintain a stable radiation pattern [3][4]. One solution that meets these requirements is the use of Dielectric Resonator Antenna (DRA) [5]. DRAs has showed themselves to be ideal candidates for various applications [6][7] by offering numerous benefits including design simplicity, wider bandwidth [5] compared to other conventional antennas and simple coupling schemes [8][5]. Moreover, the DRA performances can be simply controlled by choosing the suitable dielectric constant of the resonator material and also its dimensions [9]. A considerable interest of research has been dedicated to the study of DRAs and it has been proved that dielectric blocks of cylindrical [10], rectangular parallelepiped [11], hemispherical [12], equilateral triangular [13] shapes can be designed to radiate through suitable choices of feed location and dimensions. Different types of feeding techniques such as microstrip lines [14], dielectric image line [15], waveguide [16], coplanar slotted waveguide [17], slot coupled DRA [18][19] and hybrid coupler technique [20] have been proposed. However, one major disadvantage of the DRA is their limited bandwidth. For a single-mode excitation, the DRA bandwidth is always below 10% [5], which is not sufficient for numerous wideband applications. To overcome this limitation, various bandwidth enhancement techniques have been investigated in the literature such as optimizing the feeding mechanisms and DRA parameters [21]. Z. Rahimian has examined in [22] two circularly polarized rectangular dielectric resonator antennas (RDRAs) for wideband applications, using a 45° rotated branch-line

* Corresponding author.
E-mail addresses: kaoutar.allabouche1@gmail.com, kaoutar.allabouche@usmba.ac.ma (K. Allabouche).

https://doi.org/10.1016/j.rineng.2024.102415
Received 15 April 2024; Received in revised form 6 June 2024; Accepted 11 June 2024
Available online 14 June 2024

coupler, located below the hollow RDRA with two tapered excitation strips connected to sidewall of RDRA, to excite two degenerate TE111 modes. Adopting a multi-permittivity structure is another recent technique that has been studied in [23] which suggested a cylindrical dielectric resonator antenna (CDRA) with two different permittivity materials for wideband applications. Stacking of DRAs [24][25], inserting an air gap and pierce through slots in the DR to lower the Q-factor [26][27] and changing the DRA shape [28][29][30], are some other techniques that has been also studied. In this regard, the last technique has been analyzed in [31] by proposing a wideband half split cylindrical dielectric resonator antenna using coaxial probe feed technique. In another study, the design of high-resistivity silicon-based dielectric resonant antennas using microelectromechanical system (MEMS) technology was addressed in [32]. This approach presented potential advancements in antenna design and manufacturing processes. Furthermore, a research endeavor described in [33] introduced a straightforward method to decouple signals in a set of dielectric patch antennas (DPA array). This method enabled the simultaneous excitation of TM40 and TE42 modes within the DPA structure, thereby enhancing the overall antenna performance. Complementing these efforts, a novel dual wideband mushroom-shaped antenna design was proposed for operation across sub-6-GHz and mm-wave frequency bands [34]. This design incorporated a cavity to improve bandwidth at sub-6-GHz frequencies, offering potential applications in various wireless communication systems. Moreover, advancements in dielectric decoupling technology for CP MIMO antenna systems were investigated in [35]. This research integrated a dielectric decoupler with a polarizer, enhancing circular polarization characteristics and improving antenna performance in complex communication environments. Finally, a water dielectric resonator antenna (DRA) with reconfiguration and broadband characteristics was presented in a study described in [36]. This innovative design could potentially offer significant improvements in antenna versatility and performance across a range of operating conditions. The culmination of our research has yielded promising results in terms of bandwidth optimization. However, challenges regarding radiation pattern stability and compactness persist. Thus, our work aims to address these issues by ensuring comprehensive coverage of the UMTS and wireless DECT phone bands (250 MHz) while maintaining consistent radiation pattern stability. Additionally, our approach offers a third advantage: the compactness of the elementary antenna. By using high permittivity materials and optimizing the spacing between elements to $\frac{\lambda}{4}$, we minimize the physical footprint of the array antenna. Moreover, to validate our proposed approach for bandwidth enhancement, a prototype has been meticulously fabricated and tested, providing tangible evidence of its effectiveness. These efforts underscore our commitment to meeting the diverse requirements of modern wireless communication systems in a straightforward manner.

2. Antenna design & optimization

2.1. Methodological approach on antenna geometry for broadband achievement

Dielectric Resonators (DRs) have been extensively studied for antenna array applications. This technology exhibits a high efficiency but usually has a limited bandwidth, when using high dielectric permittivity materials [7]. In this section, we detail the iterative process that led to the final antenna structure, highlighting the steps taken to achieve optimal geometry. Our investigation begins with a meticulous analysis of diverse configurations, each presenting iterative modifications to the basic cylindrical resonator. The overarching objective is the attainment of a significantly widened bandwidth. This systematic exploration is undertaken with the specific aim of discerning the nuanced variations in bandwidth achievable through the use of a cylindrical dielectric resonator (CDR) as a fundamental shape. Through rigorous experimentation and analysis, we endeavor to illuminate the intricate pathways leading to enhanced bandwidth performance. The cylindrical DR offers the possibility to be excited with three fundamental modes indicated as $HEM11\delta$, $TE01\delta$, and $TM01\delta$, which makes it an appropriate candidate for multiband, wideband or diversity applications. These modes are given by the following equations [5]:

- The $\mathrm{HEM}_{11\delta}$ mode:

$$K_0 R = \frac{6.324}{\sqrt{\varepsilon_r + 1}} \left[0.27 + 0.36 \left(\frac{R}{2H} \right) + 0.02 \left(\frac{R}{2H} \right)^2 \right] \tag{1}$$

- The $\mathrm{TM}_{01\delta}$ mode:

$$K_0 R = \frac{\sqrt{3.83^2 + \left(\pi \frac{R}{2H} \right)^2}}{\sqrt{\varepsilon_r + 2}} \tag{2}$$

- The $\mathrm{TE}_{01\delta}$ mode.

$$K_0 R = \frac{2.327}{\sqrt{\varepsilon_r + 1}} \left[1 + 0.2123 \left(\frac{R}{H} \right) + 0.0089 \left(\frac{R}{H} \right)^2 \right] \tag{3}$$

where $K_0 = \frac{2\pi f_0}{c}$ denotes the free space wavenumber at the resonant frequency f_0 and c is the speed of light in free space. R and H are the cylindrical DR's radius and height, respectively, and are extracted from the equations mentioned above. ε_r is the permittivity of the dielectric resonator.

The decision to adopt the cylindrical shape for the DR was based on our previous research work outlined in [10]. Our findings therein showcased the benefits of the HEM mode excitation in the CDR, notably its resilience and insensitivity to external environmental factors. Henceforth, we initiate modifications in both geometry and permittivity across distinct segments of the cylindrical resonator. Fig. 1 illustrates the various studied structures:

Step 1: Serving as the reference, featuring an antenna with a simple cylindrical dielectric resonator, with a height of $h_{\mathrm{RD}} = 14.5$ mm, a radius of $R_{\max} = 14.5$ mm, a permittivity of $\varepsilon_{\mathrm{RD}} = 30$, and powered by a 50Ω microstrip feedline.

Step 2: This entails Cylindrical Ring Dielectric Resonator. The transition to this configuration is motivated by the objective of reducing the effective permittivity of the cylinder, thereby facilitating bandwidth enhancement. The radius of the inner cylinder, which has been replaced with air, is denoted as $R_{\mathrm{int}} = 4.6$ mm.

Step 3 & 4: For this last iteration, we divided the cylindrical ring into four symmetrical pieces (camembert-shaped resonators), for which we changed the permittivity values to excite adjacent modes, in order to broaden the operating bandwidth. Additionally, an air gap was inserted between each pair of dielectric resonator pieces to further broaden the bandwidth. A study was conducted to investigate the effect of rotating this air gap on the bandwidth, and the results will be presented shortly. The new optimized dimensions of the antenna are as follows: $\alpha = 60°$, $d = 1.1$ mm, $h_{\mathrm{RD}} = 15.5$ mm, $R_{\mathrm{ext}} = 15.8$ mm, and $R_{\mathrm{int}} = 4.6$ mm. The same permittivity values as the previous structure were maintained. All the configurations were simulated using HFSS software, employing a Rogers RO4003 substrate measuring 10×10 cm^2, with the following specifications: dielectric permittivity $\varepsilon_r = 3.32$, $\tan\delta = 0.0027$, and a height of $h = 1.524$ mm. A preliminary electromagnetic simulation was performed for the different configurations previously described. Fig. 2 shows how the reflection coefficient changes with each structure. It was noticed that the bandwidth was relatively narrow, about 5%, with the simple cylindrical dielectric resonator (CDR). Upon transitioning to the cylindrical ring (2$^{\mathrm{nd}}$ configuration), a slight improvement in bandwidth was noted. However, in the 3rd configuration, another mode emerged, but it wasn't well excited, so the bandwidth remained insignificant according to the −10 dB bandwidth criterion. Finally, with the last configuration, we achieved a significant bandwidth, reaching

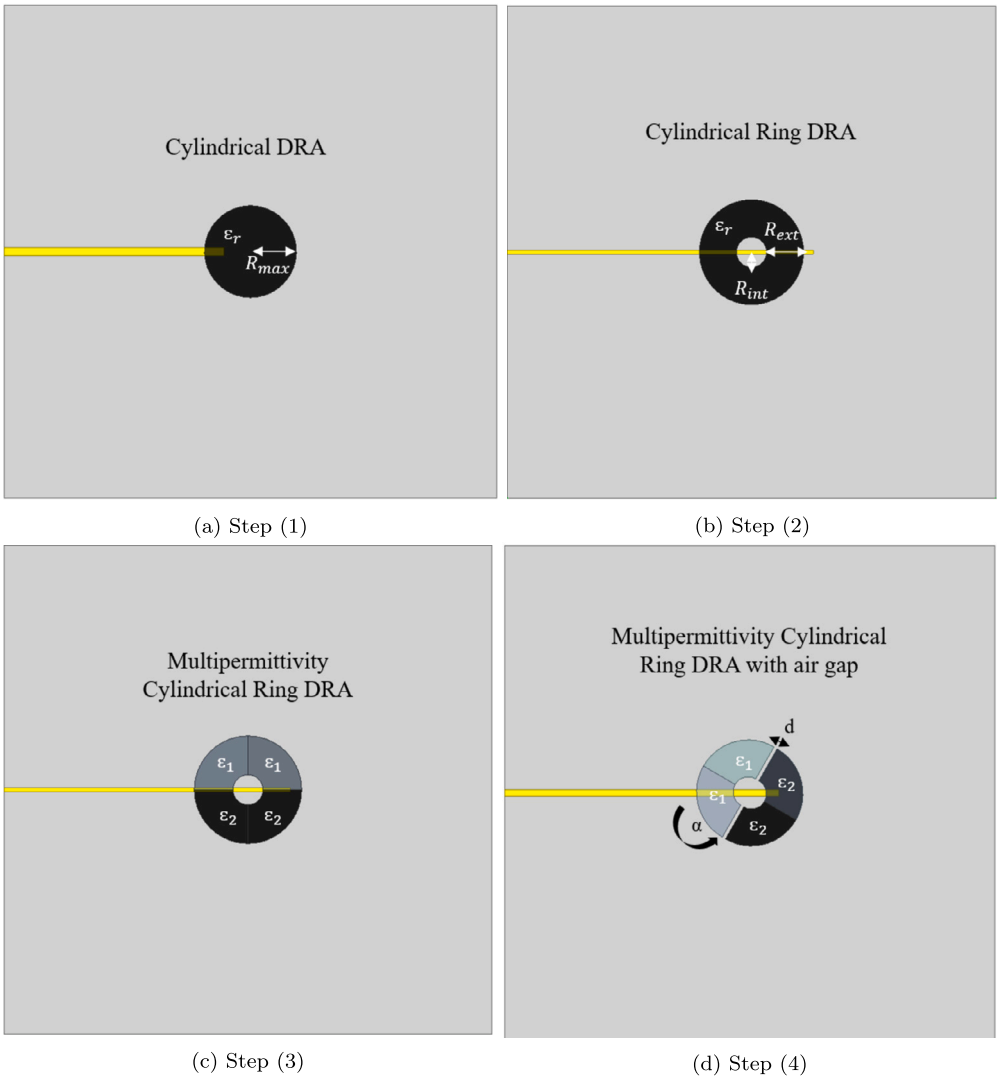

(a) Step (1) (b) Step (2)

(c) Step (3) (d) Step (4)

Fig. 1. Steps to achieve the multi-permittivity camembert-shaped DRA with rotation of the Air Gap.

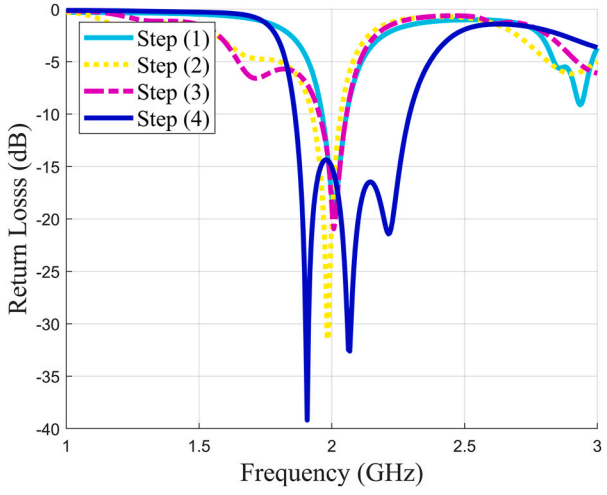

Fig. 2. Return Loss corresponding to the four studied configurations.

20% around 2 GHz, with excellent impedance matching. This improvement was mainly due to the introduction of an air gap between the camembert dielectric elements and rotating it by an angle $\alpha = 60°$ relative to the feed line. The permittivity of the dielectric resonator emerges as the most crucial parameter in this structure, as it directly influences the resonance frequency and bandwidth. As discussed in the introduction review, an increase in the permittivity of the dielectric resonator will shift the resonance frequency towards lower bands. To characterize the influence of the DR's permittivity on the resonance frequency and the bandwidth of the proposed structure, we considered three possible scenarios: in the first case, the camembert resonators with the same permittivities are placed side by side. Concerning the second configuration, the elements with different permittivities are placed side by side, and finally, in the third configuration, all elements possess the same dielectric permittivity value. Fig. 3 illustrates these various simulated scenarios. The simulation results for the three configurations are illustrated in Fig. 4. It can be noticed that incorporating dual permittivities, $\varepsilon_1 = 25$ and $\varepsilon_2 = 30$, within the resonator, regardless of their spatial arrangement, leads to a significant enhancement in bandwidth compared to using a single permittivity. We have previously observed that the introduction of an air gap between the camembert resonators allows the widening of the antenna's bandwidth. To demonstrate this characteristic, we conducted a parametric study on this parameter, by varying its length from 0.1 mm to 2.1 mm with a step of 0.2 mm. The effect of the air gap width, denoted d, on the reflection coefficient of the proposed antenna is illustrated in Fig. 5. According to this figure, it can be observed that the gap width is a critical parameter governing the antenna bandwidth. Indeed, for $d = 1.1$ mm, the bandwidth

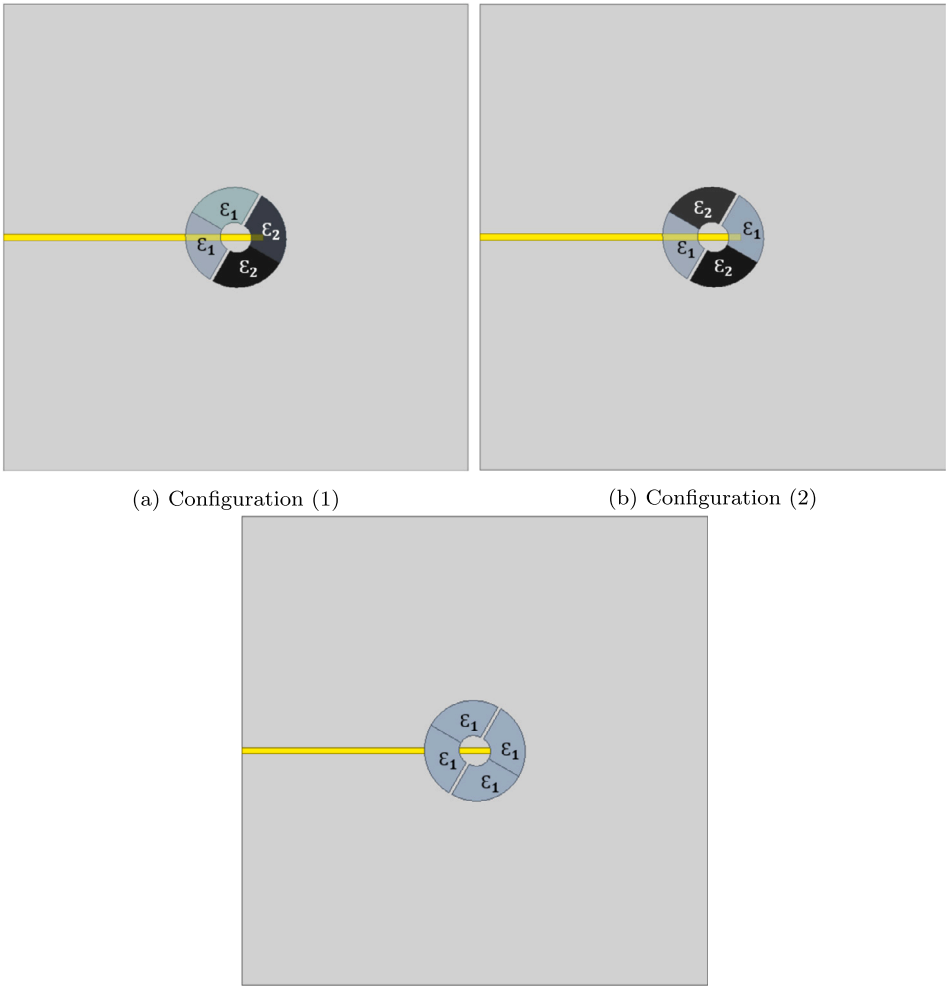

(a) Configuration (1) (b) Configuration (2)

(c) Configuration (3)

Fig. 3. Studied Structure with Different Permittivity Configurations.

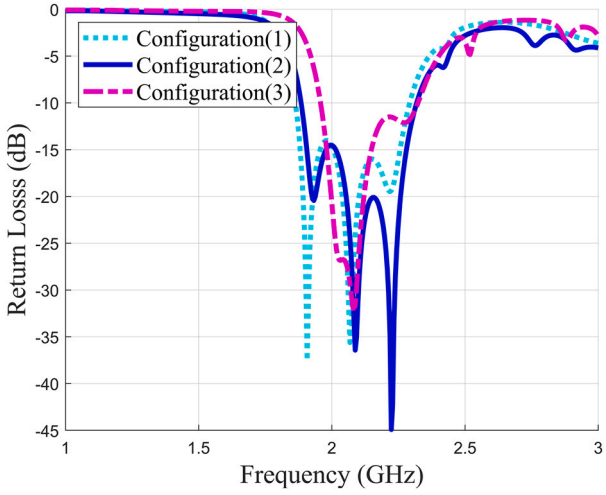

Fig. 4. Parametric Analysis of the DR Permittivity effect on the Reflection Coefficient.

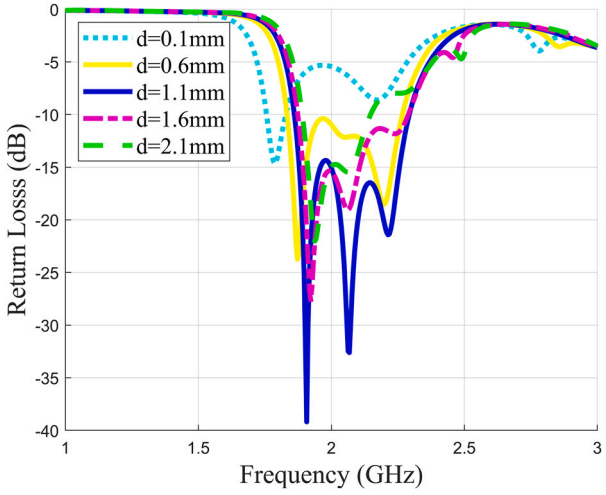

Fig. 5. Parametric Examination of the Return loss for various width d values.

reaches 20% around 2 GHz. Another crucial parameter affecting the bandwidth of the structure is the air gap rotation angle α relative to the center of the resonator. We conducted an analysis to assess its impact on the impedance bandwidth. The outcomes of this investigation are depicted in Fig. 6. The angle α ranges from 40° to 80° with a step of 10°. It is notable from the plotted curves that the widest bandwidth was achieved at a value of $\alpha = 60°$. To verify the excited mode within the proposed structure, a simulation of the surface electrical and magnetic field distributions at the operating frequency 2 GHz has been carried

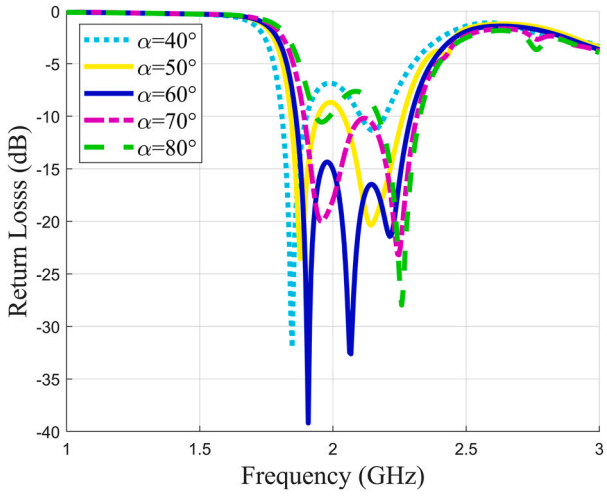

Fig. 6. S-Parameters response of the proposed antenna for different Angle α values.

out. The field distribution of the fundamental HEM mode inside the resonator antenna is sketched in Fig. 7. The electric field vectors (E) exhibit a concentration along the edges of the segmented ring resonator and within the air gap, highlighting the influence of the discontinuities introduced by the air gap. This concentration indicates higher electric field intensities at the boundaries of each segment. The magnetic field vectors (H), on the other hand, show a redistribution pattern influenced by the segmentation and the presence of air gaps. The continuity of the magnetic fields is disrupted, resulting in more concentrated magnetic field lines around the interfaces between the segments and across the air gap. These patterns illustrate the perturbation in the electromagnetic fields caused by the segmentation and the air gap, which in turn affect the resonance mode. Despite the discontinuities due to the air gap within the resonator segments, the HEM mode has been successfully excited. We can notice, also that the two fields are confined inside the resonator. Furthermore, the magnetic field is maximum in the azimuth plane at $\phi = 0^{\circ}$, while the electric field is maximum in the plane at $\phi = 90^{\circ}$. After the parametric studies, the final structure of the multi-permittivity camembert dielectric resonator antenna is depicted in Fig. 8.

The DR antenna is characterized by an outer radius R_{ext}, an inner radius R_{int}, a height h_{RD}, and two permittivities ε_1 and ε_2. It is placed above a ground plane with a width $W = 10$ cm, a length $L = 10$ cm, and coupled through a 50Ω characteristic impedance microstrip line of length L_f and width W_f. The DRA is mounted on a Rogers 4003 substrate with a length L, a width W, a thickness h, a dielectric constant of 3.32, and a loss tangent of 0.0027. The air gap separating the camembert resonators is characterized by its width d and its rotation angle α. From the parametric studies, we have extracted the optimized parameters of the proposed broadband antenna. Referring to results previously presented, the optimized values are depicted in Table 1. The decision to adopt the configuration where camembert resonators with the same permittivity are placed side by side was made for facilitating manufacturing purpose.

Table 1
Optimized geometric dimensions of the proposed antenna.

Element	Parameter	Value
Dielectric Substrate	W	100 mm
	L	100 mm
	h	1.524 mm
	ε_r	3.3
Dielectric Resonator	R_{ext}	15.8 mm
	R_{int}	4.6 mm
	h_{RD}	15.5 mm
	ε_1	25
	ε_2	30
Feed Line	W_f	2 mm
	L_f	84 mm
Air gap	d	1.1 mm
	α	60°

3. Experimental assessment & results discussion

3.1. Dielectric resonators manufacturing: printing process and characterization equations

The Dielectric Resonators were fabricated by Nanoe [37], a French company based in Paris, specializing in the manufacturing of filaments for $3D$ printing. Recently, ceramic and meta 3D printing technique named Zetamix and based on Fuse Filament Fabrication (FFF) has been introduced by Nanoe [37]. It allows the creation of complex ceramic shapes in alumina, zirconia and also steel by FFF. In this process, a ceramic/thermoplastic filament with very high loadings of ceramic is printed on standard printer, by melting the filament through a deposition nozzle, and the part is produced layer by layer to form a 3D printed green part. This part is then debinded (by chemically removing the binder) and sintered (heat treated at 1400– 1500°C) to obtain a dense ceramic part. Typical densities of ceramics are around 99% after sintering. This technology makes ceramic 3D printing both simple and affordable, while allowing shapes of an unprecedented level of complexity. Materials available with this technology are Alumina and Zirconia, which exhibit very interesting dielectric properties with permittivity of respectively $\varepsilon_r = 10$ and 30, and low loss with $\tan\delta = 0.001$.

Various characterization approaches have been explored in achieving the desired permittivities. Among these methods, the Maxwell-Garnett, Upper Weiner bound, and Lower Weiner bound equations [38]. The Maxwell-Garnett equation estimates the effective permittivity of a composite by considering the volume fraction and permittivity of its constituents, assuming homogeneity and isotropy. The Upper Weiner bound provides a conservative upper limit for the effective permittivity, applicable when inclusions have significantly higher permittivity or conductivity than the matrix. Conversely, the Lower Weiner bound offers a conservative lower limit for materials where inclusions have lower permittivity or are insulating. These equations play a crucial role in characterizing composite materials and are described in detail below:

- Maxwell Garnett:

$$\varepsilon_{\text{eff}} = \varepsilon_m \left(\frac{\varepsilon_i + 2\varepsilon_m + 2C(\varepsilon_i - \varepsilon_m)}{2\varepsilon_m + \varepsilon_i + C(\varepsilon_i - \varepsilon_m)} \right) \tag{4}$$

- Wiener Upper Bound:

$$\varepsilon_{\max} = \varepsilon_i C + (1 - C)\varepsilon_m \tag{5}$$

- Wiener Lower Bound:

$$\varepsilon_{\min} = \frac{\varepsilon_m \varepsilon_i}{\varepsilon_m C + (1 - C)\varepsilon_i} \tag{6}$$

With: $\varepsilon_m = 1$ is the air permittivity and $\varepsilon_i = 33$ is the zirconia permittivity. According to the inverse Maxwell-Garnett law, which enables the permittivity calculation based on the material's filling ratio, pieces with different permittivities were printed using the same filament.

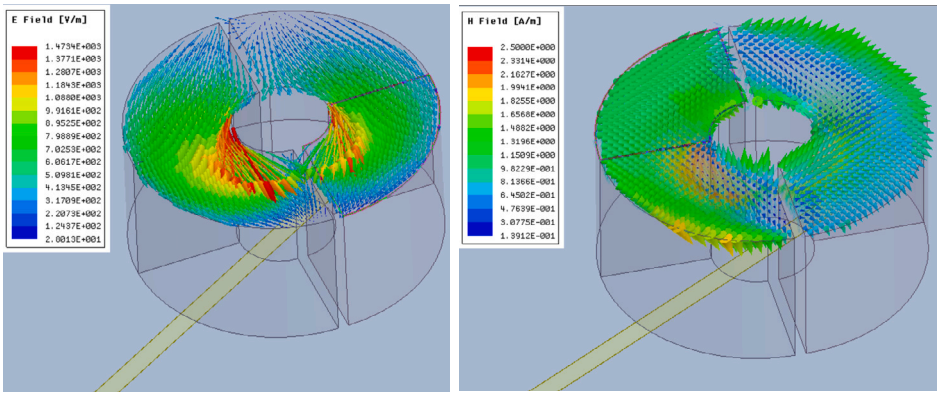

(a) E-Field (b) H-Field

Fig. 7. Field Distribution inside of the proposed antenna excited at 2 GHz.

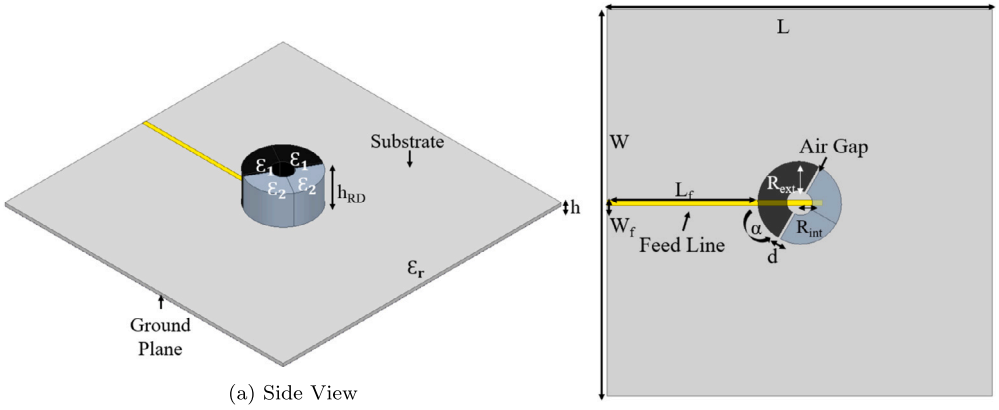

(a) Side View (b) Top View

Fig. 8. Geometric Structure of the Proposed Camembert-Inspired DRA.

During filament deposition, a "liant" was employed in conjunction with the ceramic material. The 'Liant' is an essential material for the shaping process. Subsequent to printing, the pieces underwent a chemical treatment, known as debinding, in an acetone bath to remove the 'Liant'. Finally, sintering involves "cooking" the resonator at very high temperatures (1475˚C). The oven increases its heating temperature by 50˚C per hour. Through sintering, the piece densifies and acquires its final mechanical properties. Fig. 9 demonstrates the impact of filling ratio on the resonator's permittivity using the three characterization methodologies. Hence, the resonators were fabricated based on the Maxwell-Garnett equation as outlined below:

- for a permittivity of 25, the filling ratio is 97.2%.
- for a permittivity of 30, the filling ratio is 99.1%.

A photograph of the fabricated Resonators is presented in Fig. 10. The accomplishment of the two different permittivities for the camembert resonators was achieved through meticulous adjustment of the filling ratio.

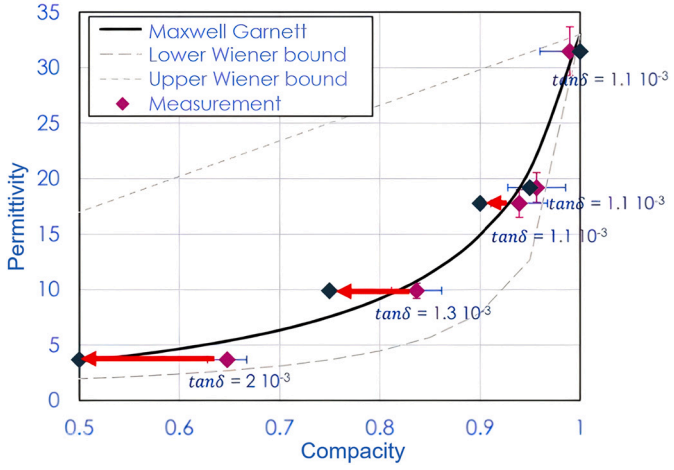

Fig. 9. DR permittivity versus compacity for the three characterizing equations.

3.2. Analysis of a 4x4 antenna array configuration

The preceding study enabled us to synthesize and design a novel multi-permittivity antenna topology based on horizontal stratification for broadband applications. To validate this design concept, a prototype antenna has been fabricated and tested. The broadband array antenna is printed on a 1.524-mm-thick RO4003C substrate with a relative permittivity of 3.38 and a loss tangent of 0.0027. An additional interesting feature of this proposed array antenna design is the spacing between the radiating elements, which is equal to $\lambda/4$. Subsequently, we will describe the designed array and assess its radiation performance. In pursuit of achieving a radiation pattern characterized

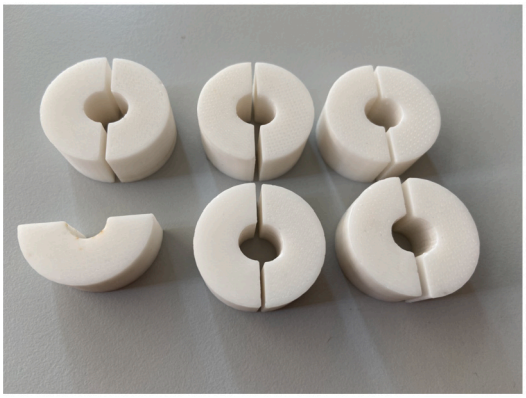

Fig. 10. Photograph of the Fabricated Dielectric Resonators.

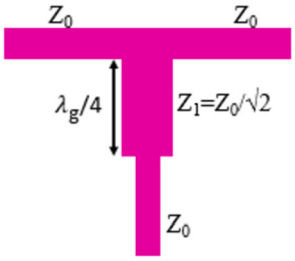

Fig. 11. T-junction power divider.

by a single lobe oriented parallel to the alignment plane of the antenna array, the spacing between each pair of neighboring radiating elements was set to 0.25λ, where λ denotes the guided wavelength. To feed our four-element antenna array, we employed a T-junction power divider, as depicted in Fig. 11. The port impedance is set to 50 Ω, and the microstrip lines beneath the four radiating elements must likewise exhibit the same characteristic impedance. Building upon this premise and leveraging the T-junction divider, we constructed our feeding network. The widths of the microstrip lines at various levels were calculated using the Macros tool of the CST software. It is imperative to highlight that the operating frequency and geometric parameters of the resonator were derived from the final configuration outlined in the preceding section. Using the optimized parameters in Table 1, the proposed array antenna was fabricated for validation.

Fig. 12 shows a photo of the prototype connected to the VNA and in the anechoic chamber. The prototype antenna is constructed using the dielectric resonators, and a T-junction power divider was employed to feed our four-element array antenna. The dielectric constants of the 3-D printing filaments are $\varepsilon_1 = 25$ and $\varepsilon_2 = 30$ with a loss tangent of 0.001 at 2 GHz, respectively. Fig. 13 depicts the simulated and measured reflection coefficient of the proposed 4×4 array antenna. It can be observed that the impedance bandwidth ($|S_{11}| < -10$ dB) can cover the frequency band of $1.86 - 2.3$ GHz, representing a relative bandwidth of 20%. A remarkably good impedance matching is observed across the bandwidth, reaching as low as −33 dB. The structure is capable of covering wireless DECT phone bands around 1.9 GHz and the UMTS mobile phone band around 2.1 GHz. Additionally, the measured $|S_{11}|$ curve shows reasonable agreement with the simulated one. Fig. 14 gives the measured and simulated antenna gains, which show reasonable consistency between each other. In the frequency band of $1.8 - 2.2$ GHz, the measured antenna gain varies between 5 and 10 dBi, whereas the simulated counterpart changes from 7 to 10 dBi. The measured total antenna efficiency considering impedance mismatch is also given in the inset of Fig. 15. Over the frequency band $1.8 - 2.2$ GHz, the total efficiency has a maximum value of 99%. The variation in the radiation patterns of the proposed structure is shown in Fig. 16. A broadside radiation pattern is observed, with a maximum gain of 10 dBi along the axis of the resonator's rotation. The radiation pattern is symmetrical in the xz plane. Additionally, as illustrated in Fig. 16, the measured radiation pattern exhibits excellent stability across the entire bandwidth (from 1.8 GHz to 2.4 GHz) for both $\phi = 90°$ and $\phi = 0°$.

Performance comparisons between the proposed Broadband Dielectric Resonator Antenna and the previously reported similar works are listed in Table 2. It can be noticed that the proposed antenna exhibits an improved bandwidth with a very lower profile compared to the other antennas. Although the bandwidth of the proposed prototype antenna is narrower than the antennas reported in [35], [36], and [40], it offers advantages in terms of compactness, higher efficiency, high gain, and good radiation pattern stability versus frequency. In summary, the proposed multi-permittivity antenna showcases high efficiency, compact size, low profile and stable radiation patterns all overs the frequency band of interest, when compared to conventional antennas. Finally, another important feature of this design is the center-to-center spacing between the adjacent elements, which is equal to 0.25λ without any decoupling method.

4. Conclusion

This letter presents a novel compact wideband Camembert-Inspired Dielectric Resonator Antenna (DRA) operating at 2 GHz, designed for mobile communication applications. The proposed multi-permittivity DRA achieves broadside radiation with an improved impedance bandwidth of approximately 20%. Furthermore, it maintains excellent stability in terms of the radiation pattern across the entire frequency band of interest. The design also offers the advantages of compactness, high efficiency, and high gain. Additionally, a 1×4 DRA array was fabricated using high relative-permittivity materials (dielectric constants of 25 and 30), providing a low-profile feature to the proposed design. The strong agreement between measurement and simulation results indicates that this design holds significant promise for mobile communication and wireless DETC applications.

CRediT authorship contribution statement

Kaoutar Allabouche: Writing – original draft, Validation, Software, Methodology, Investigation, Formal analysis, Data curation. **Fabien Ferrero:** Supervision, Resources, Funding acquisition. **Hugo Bernadac:** Validation. **Jean-Marc Ribero:** Supervision. **Leonardo Lizzi:** Supervision. **Najiba El Amrani El Idrissi:** Supervision. **Mohammed Jorio:** Supervision. **Guillaume De Calan:** Validation. **Julien Sourice:** Validation.

Declaration of competing interest

The authors declare the following financial interests/personal relationships which may be considered as potential competing interests: ALLABOUCHE KAOUTAR reports financial support was provided by université cote d'azur.

Data availability

No data was used for the research described in the article.

Acknowledgement

The authors would like to thank the LEAT for its tremendous support.

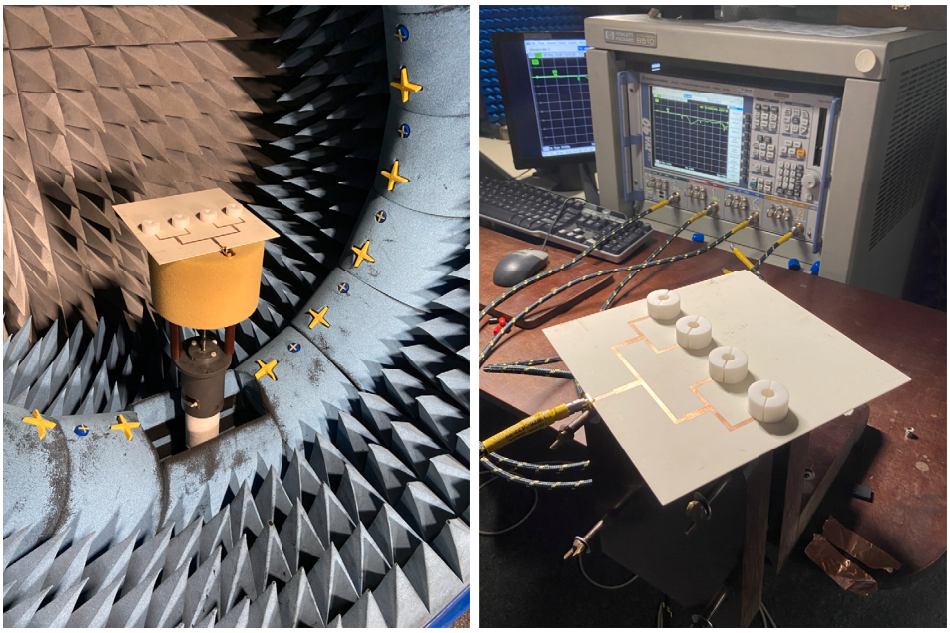

(a) Prototype in the Anechoic Chamber (b) Prototype connected to the VNA

Fig. 12. Photograph of the fabricated prototype.

Table 2
Performance comparisons of the proposed wideband antenna to previous reported work.

Ref	Freq. (GHz)	Ant. Type	Decoup. Method	Array Elmt. Num	Dim. (λ^2)	BW (%)	PG (dBi)	Effic. (%)	Rad Patt. Stability
[33]	5.5	Monolithic DPA	Air slots	1*4	0.06	16.9	8.9	98.05	Yes
[35]	10	DRA	Dielectric Decoupler	1*2	0.77x0.19	21.7	4-5	>80	-
[36]	2.45	CDRA	-	1	0.3x0.22	22	3-4	>70	No
[39]	30	Conical DRA	-	1	0.7x1.27	16.6	11.3	>71	-
[40]	3.4	CDRA	-	1	0.31x0.15	30	3.2-3.5	>85	No
[41]	5	RDRA	-	1*4	0.41x0.41	17	13.55	-	Yes
[42]	2.44	RDRA	-	1*4	0.14x012	16.9	6.8	-	-
[43]	7.5	CDRA	-	1*4	0.1x0.15	7	10	>63	-
[44]	7.56	CDRA	Split Ring resonator	1*2	0.1x0.15	8.8	4.5	>63	-
Prop	2	Multi-permittivity CDRA	N.A	1*4	0.1x0.14	20	10	99	Yes

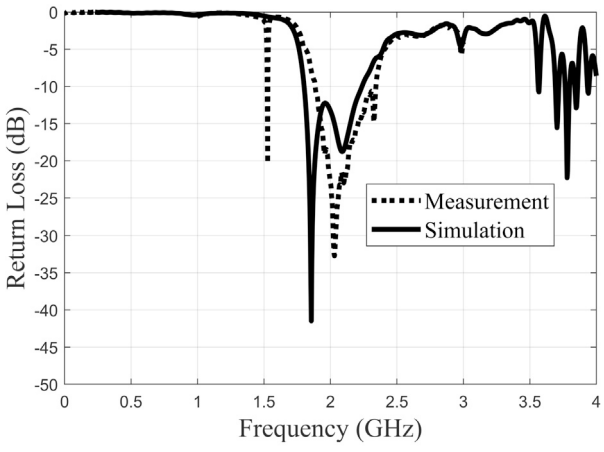

Fig. 13. Comparison of return loss of fabricated and simulated proposed antenna.

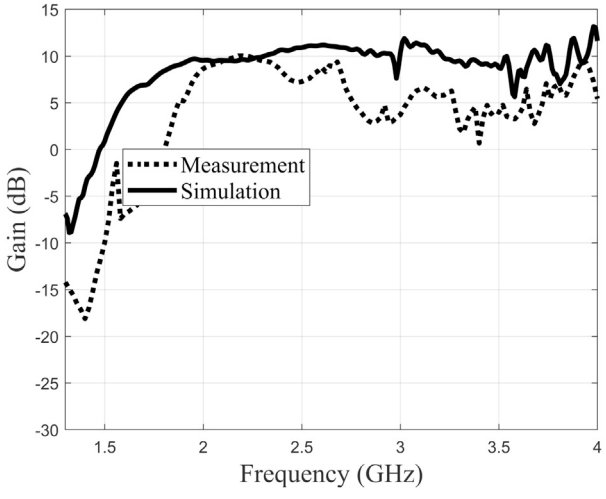

Fig. 14. Total Gain versus frequency.

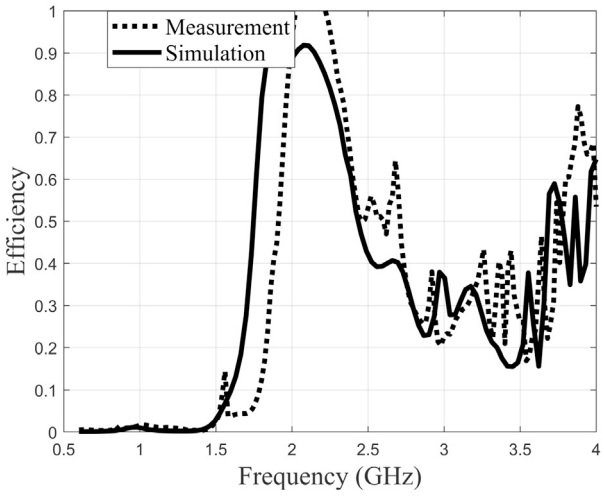

Fig. 15. Total Efficiency versus frequency of the proposed antenna.

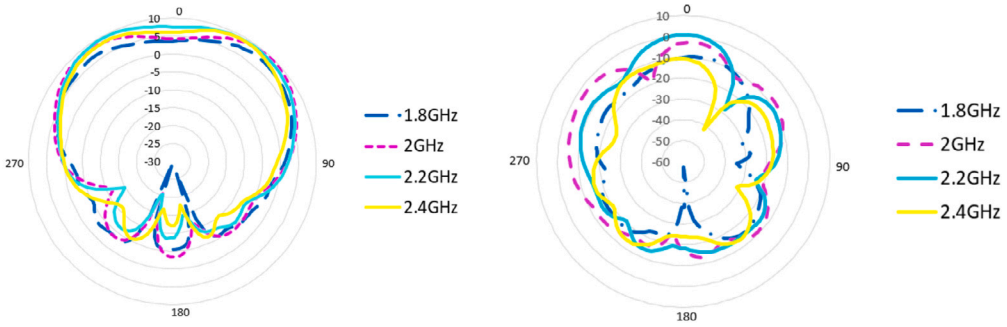

(a) Polar-V at $\phi = 90°$ (b) Polar-V at $\phi = 0°$

Fig. 16. Measured 2D Radiation Pattern versus frequency.

References

[1] A. Baz, D. Jansari, S.P. Lavadiya, S.K. Patel, Miniaturized and high gain circularly slotted 4×4 MIMO antenna with diversity performance analysis for 5G/Wi-Fi/WLAN wireless communication applications, Results Eng. (ISSN 2590-1230) 20 (2023) 101505.

[2] U. Patel, T. Upadhyaya, V. Sorathiya, K. Pandya, A. Alwabli, K. Dave, N.F. Soliman, W. El-Shafai, Split ring resonator geometry inspired crossed flower shaped fractal antenna for satellite and 5G communication applications, Results Eng. (ISSN 2590-1230) 22 (2024) 102110.

[3] J.K. Fujimoto, J.R. James, Mobile Antenna Systems Handbook, Artech House, Boston, UK, 1994.

[4] K.L. Wong, Planar Antennas for Wireless Communications, John Wiley & Sons, USA, 2003.

[5] K.M. Luk, K.W. Leung, Dielectric Resonator Antennas, Research Studies Press Ltd., Baldock, Hertfordshire, England, 2003.

[6] K. Allabouche, T. Mazri, M. Jorio, N. El Amrani El Idrissi, Comparative analysis of microstrip and dielectric resonator antennas for UMTS application, Int. J. Commun. Antenna Propag. 5 (1) (2015).

[7] K. Allabouche, F. Ferrero, J.-M. Ribero, et al., Compact high-Q slot loaded dielectric resonator filtering antenna for LoRa applications, AEÜ, Int. J. Electron. Commun. 175 (2024) 155078.

[8] A. Petosa, Dielectric Resonator Antennas Handbook, Artech House Inc, 2007.

[9] S.A. Long, M.W. McAllister, L.C. Shen, The resonant dielectric cavity antenna, IEEE Trans. Antennas Propag. 31 (3) (1983) 406–412.

[10] K. Allabouche, F. Ferrero, J-M. Ribero, L. Lizzi, M. Jorio, N. El Idrissi, Proximity effect of metallic environments on cylindrical dielectric resonator antenna for smart metering applications, Int. J. Microw. Opt. Technol. 12 (2017) 249–258, No. 4.

[11] M.W. McAllister, S.A. Long, Rectangular dielectric resonator antenna, IEEE Electron. Lett. 19 (1983) 218–219.

[12] M. McAllister, S.A. Long, Resonant hemispherical dielectric antenna, IEEE Electron. Lett. 20 (1984) 657–659.

[13] R.K. Mongia, Half-split dielectric resonator placed on metallic plane for antenna applications, IEEE Electron. Lett. 25 (1989) 462–464.

[14] F.H. Wee, et al., Investigation of the characteristics of barium strontium titanate (BST) dielectric resonator ceramic loaded on array antennas, Prog. Electromagn. Res. 121 (2011) 181–213.

[15] A. Al-Zoubi, A.A. Kishk, A.W. Glisson, Analysis and design of a rectangular dielectric resonator antenna fed by dielectric image line through narrow slots, Prog. Electromagn. Res. 77 (2007) 379–390.

[16] R.Q. Lee, R.N. Simons, Bandwidth enhancement of dielectric resonator antennas, in: Antennas and Propagation Society International Symposium, AP-S, Digest, 1993.

[17] I.A. Eshrah, et al., Theory and implementation of dielectric resonator antenna excited by a waveguide slot, IEEE Trans. Antennas Propag. 53 (1) (2005) 483–494.

[18] E. Lee, M.L.C. Ong, Aperture coupled, differentially fed DRAs, in: Asia Pacific Microwave Conference, 2009, pp. 2781–2784.

[19] A. Buerkle, K. Sarabandi, H. Mosallaei, Compact slot and dielectric resonator antenna with dual resonance, broadband characteristics, IEEE Trans. Antennas Propag. 53 (3) (2005) 1020–1024.

[20] Kah-Wee Khoo, Wideband circularly polarized dielectric resonator antenna, IEEE Trans. Antennas Propag. 55 (7) (2007).

[21] A. Kishk, Y. Yin, A.W. Glisson, Conical dielectric resonator antenna for wideband applications, IEEE Trans. Antennas Propag. 50 (2002) 469–474.

[22] Z. Rahimian, S. Nikmehr, A. Pourziad, Circularly polarized rectangular dielectric resonator antennas with branch-line coupler for wideband applications, AEÜ, Int. J. Electron. Commun. 69 (2015) 169–175.

[23] Ubaid Ullah, et al., Design of a novel dielectric resonator antenna using Mg-TiO3–CoTiO3 for wideband applications, Mater. Des. 85 (2015) 396–403.

[24] A.G. Walsh, S.D. Young, S.A. Long, An investigation of stacked and embedded Cylindrical Dielectric Resonator Antennas, IEEE Antennas Wirel. Propag. Lett. 5 (2006) 130–133.

[25] B. Sahu, et al., Dual segment rectangular dielectric resonator antenna with metamaterial for improvement of bandwidth and gain, Int. J. RF Microw. Comput.-Aided Eng. 24 (2014) 646–655.

[26] L.Z. Thamae, Z. Wu, Broadband bowtie dielectric resonator antenna, IEEE Trans. Antennas Propag. 58 (2010) 3707–3710.

[27] B. Mukherjee, et al., A novel cheeseholes type hemispherical dielectric resonator antenna for wireless applications, in: Proceedings of the IEEE EuMC, Germany, 2013.

[28] R. Chair, et al., Wide band flipped staired pyramid dielectric resonator antenna, Electron. Lett. 40 (2004) 581–582.

[29] A.A. Kishk, Wide-band truncated tetrahedron dielectric resonator antenna excited by a coaxial probe, IEEE Trans. Antennas Propag. 51 (2003) 2913–2917.
[30] S. Keyrouz, D. Caratelli, Dielectric resonator antennas: basic concepts, design guidelines, and recent developments at millimeter-wave frequencies, Int. J. Antennas Propag. 2016 (2016) 6075680.
[31] P. Ranjan, R.K. Gangwar, Probe feed half split cylindrical dielectric resonator antenna for wideband applications, AEÜ, Int. J. Electron. Commun. 69 (2015) 1709–1714.
[32] Y.-S. Huang, et al., Wideband and low-profile high-resistivity silicon-based dielectric resonant antennas by loading AMC, IEEE Trans. Antennas Propag. 71 (11) (2023) 9024–9029.
[33] L.-L. Yang, et al., A wideband decoupled monolithic multielement dielectric patch antenna array with steerable beam, IEEE Antennas Wirel. Propag. Lett. 22 (9) (2023) 2235–2239.
[34] R.S. Malfajani, et al., A dual wide-band mushroom-shaped dielectric antenna for 5G sub-6-GHz and mm-wave bands, IEEE Open J. Antennas Propag. 4 (2023) 614–625.
[35] C. Yang, K.W. Leung, 3-D-printed wideband circularly polarized MIMO dielectric resonator antenna, IEEE Trans. Antennas Propag. 71 (7) (July 2023) 5675–5683.
[36] M. Wang, Q.-X. Chu, A wideband polarization-reconfigurable water dielectric resonator antenna, IEEE Antennas Wirel. Propag. Lett. 18 (2) (2019) 402–406.
[37] Nanoé, https://nanoe.com/, (Consulté le [02/12/2022]).
[38] J. Smith, et al., Analysis of composite materials using the Maxwell-Garnett equation and upper and lower weiner bounds, J. Compos. Mater. 45 (3) (2021) 321–335.
[39] E. Baldazzi, et al., A high-gain dielectric resonator antenna with plastic-based conical horn for millimeter-wave applications, IEEE Antennas Wirel. Propag. Lett. 19 (6) (2020) 949–953.
[40] T. Yang, et al., Wideband diversity cylindrical dielectric resonator antenna based on multimode resonance, IEEE Antennas Wirel. Propag. Lett. 22 (9) (2023) 2205–2209.
[41] S.-C. Tang, et al., Wideband low-profile dielectric patch antenna and array with anisotropic property, IEEE Trans. Antennas Propag. 68 (5) (2020) 4091–4096.
[42] S. Chaudhuri, et al., Wideband rectangular dielectric resonator antenna array for ISM band applications, in: 2020 IEEE Region 10 Symposium (TENSYMP), Dhaka, Bangladesh, 2020, pp. 622–625.
[43] N.K. Mishra, S. Das, D.K. Vishwakarma, Beam steered linear array of Cylindrical Dielectric Resonator Antenna, AEÜ, Int. J. Electron. Commun. 98 (2019) 106–113.
[44] N.K. Mishra, J. Acharjee, V. Sharma, C. Tamrakar, L. Dewangan, Mutual coupling reduction between the cylindrical dielectric resonator antenna using split ring resonator based structure, AEÜ, Int. J. Electron. Commun. 154 (2022).